Genetics inMedicine

www.nature.com/gim

Check for updates

ARTICLE

Heterozygous loss-of-function variants significantly expand the phenotypes associated with loss of *GDF11*

Thomas A. Ravenscroft[1,2], Jennifer B. Phillips[3], Elizabeth Fieg[4], Sameer S. Bajikar[1,2], Judy Peirce[3], Jeremy Wegner[3], Alia A. Luna[3], Eric J. Fox[3], Yi-Lin Yan[3], Jill A. Rosenfeld[1,5], Jonathan Zirin[6], Oguz Kanca[1,2], Undiagnosed Diseases Network*, Paul J. Benke[7], Eric S. Cameron[7], Vincent Strehlow[8], Konrad Platzer[8], Rami Abou Jamra[8], Chiara Klöckner[8], Matthew Osmond[9], Thomas Licata[9], Samantha Rojas[9], David Dyment[9], Josephine S. C. Chong[10], Sharyn Lincoln[11], Joan M. Stoler[11], John H. Postlethwait[3], Michael F. Wangler[1,2], Shinya Yamamoto[1,2,12], Joel Krier[4], Monte Westerfield[3] and Hugo J. Bellen[1,2,12,13]✉

PURPOSE: Growth differentiation factor 11 (GDF11) is a key signaling protein required for proper development of many organ systems. Only one prior study has associated an inherited *GDF11* variant with a dominant human disease in a family with variable craniofacial and vertebral abnormalities. Here, we expand the phenotypic spectrum associated with *GDF11* variants and document the nature of the variants.

METHODS: We present a cohort of six probands with de novo and inherited nonsense/frameshift (4/6 patients) and missense (2/6) variants in *GDF11*. We generated *gdf11* mutant zebrafish to model loss of *gdf11* phenotypes and used an overexpression screen in *Drosophila* to test variant functionality.

RESULTS: Patients with variants in *GDF11* presented with craniofacial (5/6), vertebral (5/6), neurological (6/6), visual (4/6), cardiac (3/6), auditory (3/6), and connective tissue abnormalities (3/6). *gdf11* mutant zebrafish show craniofacial abnormalities and body segmentation defects that match some patient phenotypes. Expression of the patients' variants in the fly showed that one nonsense variant in *GDF11* is a severe loss-of-function (LOF) allele whereas the missense variants in our cohort are partial LOF variants.

CONCLUSION: *GDF11* is needed for human development, particularly neuronal development, and LOF *GDF11* alleles can affect the development of numerous organs and tissues.

Genetics in Medicine (2021) 23:1889–1900; https://doi.org/10.1038/s41436-021-01216-8

INTRODUCTION

Growth differentiation factor (GDF) proteins are members of the bone morphogenetic proteins (BMP) subfamily of transforming growth factor-beta (TGF-β) ligands and are key signaling proteins for development.[1,2] Loss-of-function (LOF) variants in GDF genes are associated with disorders affecting many different organs and tissues (Supplementary Table 1). Additionally, individual LOF variants within the same GDF gene can lead to pleiotropic effects.[3,4] Pleiotropy of individual GDF genes is likely due to the complex role of these genes in the development of multiple tissues[5,6] and functional redundancies among GDF/BMP genes.[7–9]

GDF11 has three domains: a signal peptide (amino acid [AA] 1–24), a mature proprotein (AA25–298), and the TGF-β domain (AA299–407) (Fig. 2c).[10] The signal peptide localizes the protein to the plasma membrane, where Furin proteases cleave the TGF-β domain at an RXXR motif (AA295–298) allowing secretion of the mature protein containing TGF-β domain while the cleaved propeptide is retained in the membrane.[11] Secreted GDF11 binds to Activin receptors, which triggers phosphorylation of SMAD2 and subsequent translocation to the nucleus, upregulating genes required for cell differentiation and tissue patterning.[12–15] *GDF11* is broadly expressed, with expression highest in skeletal muscle, pancreas, kidney, retina, and the brain.[10,16–18] *GDF11* is expressed ubiquitously within the brain with expression highest in oligodendrocytes, oligodendrocyte precursors, and astrocytes, followed by neurons.[19] *GDF11* is most highly expressed during development and early life and its levels decline with aging.[20,21] The breadth of *GDF11* expression, coupled with high levels during pre- and postnatal developmental stages, indicates that *GDF11* may be required for proper organogenesis and homeostasis after birth.

A *GDF11* variant (NP_005802.1:p.[R298Q]) with a dominant inheritance pattern and variable penetrance and expressivity has been documented in a large family whose members presented with cleft lip/palate as well as rib and vertebral hypersegmentation.[22] The affected arginine (R) is the second arginine in the RXXR motif essential for TGF-β domain cleavage.[11] When this arginine is replaced with glutamine, the TGF-β domain is not cleaved by Furin proteases.[22] The biochemical data, coupled with the dominant inheritance pattern, suggest that this allele behaves as a dominant LOF variant.

[1]Department of Molecular and Human Genetics, Baylor College of Medicine, Houston, TX, USA. [2]Jan and Dan Duncan Neurological Research Institute, Texas Children Hospital, Houston, TX, USA. [3]Institute of Neuroscience, University of Oregon, Eugene, OR, USA. [4]Brigham and Women's Hospital, Boston, MA, USA. [5]Baylor Genetics Laboratories, Houston, TX, USA. [6]Department of Genetics, Harvard Medical School, Boston, MA, USA. [7]Joe DiMaggio Children's Hospital, Hollywood, FL, USA. [8]Institute of Human Genetics, University of Leipzig Medical Center, Leipzig, Germany. [9]Children's Hospital of Eastern Ontario, Ottawa, Ontario, Canada. [10]The Chinese University of Hong Kong-Baylor College of Medicine Joint Center of Medical Genetics, Hong Kong Special Administrative Region, The People's Republic of China. [11]Boston Children's Hospital, Boston, MA, USA. [12]Department of Neuroscience, Baylor College of Medicine, Houston, TX, USA. [13]Howard Hughes Medical Institute, Baylor College of Medicine, Houston, TX, USA. *A list of authors and their affiliations appears at the end of the paper. ✉email: hbellen@bcm.edu

Model organism studies have defined a developmental role for *GDF11*.[10,23–27] *Gdf11*-deficient (*Gdf11*$^{-/-}$) mice die within 24 hours of birth with renal and palate abnormalities.[10] The skeleton of *Gdf11*$^{-/-}$ mice exhibits an increased number of ribs, anteriorly directed homeotic transformations, posterior displacement of hindlimbs, and defective inner ear structure.[10,28] *Gdf11* is a haploinsufficient locus in mice and skeletal abnormalities are seen in heterozygous animals; *Gdf11*$^{+/-}$ mice present fewer additional ribs and less severe craniofacial abnormalities than *Gdf11*$^{-/-}$ mice indicating that the effect of GDF11 function on skeletal development is dose-dependent.[10] *Gdf11* is also required for the timing and progression of neurogenesis during the development of the spinal cord, retina, and olfactory epithelium.[23,26,29] *Gdf11*-related defects are typically attributed to aberrant *Hox* gene expression downstream of *Gdf11* signaling, which in turn causes major tissue patterning defects in development.[10]

We have identified a cohort of patients with both de novo and inherited variants in *GDF11* presenting with complex neurological, cardiovascular, connective tissue, ocular, and auditory phenotypes, in addition to the craniofacial and skeletal abnormalities previously described. Additionally, we generated a *gdf11* LOF zebrafish model and we used *Drosophila* to evaluate the function of three of the patients' *GDF11* variants.

MATERIALS AND METHODS

Human genetics

All probands were exome or genome sequenced (Supplementary Methods [SM]). All *GDF11* variants were Sanger confirmed. *GDF11* variants are mapped onto the NM_005811.5 RefSeq transcript.

Sequence alignment

Protein sequences from human GDF11 (NP_005802.1), mouse Gdf11 (NP_034402.1), zebrafish gdf11 (NP_998140.1), and *Drosophila* myo (NP_726604.1) were obtained from the National Center for Biotechnology Information (NCBI) and aligned using BoxShade (https://embnet.vital-it.ch/software/BOX_form.html).

Quantification of *GDF11* gene and protein levels from peripheral blood mononuclear cells

Peripheral blood mononuclear cell (PBMC) samples were quickly thawed at room temperature and centrifuged at 500*g* for 5 minutes at room temperature. RNA and protein were isolated and analyzed using separate protocols described in SM. The primers used to quantify gene expression are provided in SM. For western blotting standard protocols were used and are described in the SM alongside antibodies used. For enzyme-linked immunosorbent assay (ELISA) circulating GDF11 levels in plasma were quantified using the human GDF11/GDF-11 Sandwich ELISA kit (LSBio #LS-F11519) according to the manufacturer's recommendations. Plasma samples were diluted 1:1 in sample diluent before processing. Quantitative polymerase chain reaction (qPCR) was performed with one technical replicate and the ELISA was performed with three technical replicates. Center values in Fig. 1b, c represent mean.

Generation of zebrafish *gdf11* mutants

Three zebrafish indel alleles were generated using CRISPR-Cas9 (SM). We generated three different frameshift deletions: *b1407*, a 2-bp deletion in exon 1, c.374-5, resulting in an E125Vfs*15 truncation; *b1408* a 7-bp deletion in exon 3, c.922-28, creating an F308Gfs*53 truncation; and *b1396*, which has a 703-bp deletion removing the 5′UTR and most of the first exon. All alleles were confirmed by sequencing aligned to the GRCz11 reference transcript ENSDART00000066033.8. Surviving F1s for each allele were raised to adulthood and genotyped to identify heterozygotes that were then increased. Homozygous viable F2 mutants were raised to adulthood and increased to obtain larvae for the described experiments, alongside control larvae from homozygous wild-type F2 siblings.

Analysis of *gdf11* expression in zebrafish

In situ hybridization was performed as described.[30] Primers used are described in SM. Image acquisition detailed in SM.

Single-cell RNA-seq expression for *gdf11* was retrieved from the zebrafish single-cell transcriptome atlas (http://cells.ucsc.edu/?ds=zebrafish-dev). Tissue-specific assignments of cell-type identities are those previously annotated.[31]

Analysis of zebrafish craniofacial structures

Zebrafish skeletal elements were fixed and stained with Alcian blue and Alizarin red as previously described.[32] Image acquisition and statistical analysis are detailed in SM.

Fly stocks and maintenance

All fly stocks used in this study were either generated in-house or were obtained from the Bloomington Drosophila Stock Center (BDSC). All flies were reared on standard fly food and maintained at room temperature unless specified. Fly lines used are listed in SM.

Generation of *UAS-myo* and *myo-T2A-GAL4* flies

The *Drosophila melanogaster* complementary DNA (cDNA) for *myo* (isoform myo-PA, FlyBase ID: FBal0267088) was generously provided by Michael O'Connor.[33] Identification of conserved amino acids corresponding to variants in human *GDF11* (fly variant in *myo* in parenthesis): p.E306K (p.E500K), p.Y336* (p.F530*), and p.R295P (p.R489P) was done using multiple protein alignment DIOPT v6[34] via Marrvel1.2 (www.marrvel.org).[35] Mutagenesis and transgene injection were done as previously described.[36] Two independent lines were made for each injected construct, and both constructs were used in all future studies. The *myo-T2A-GAL4* allele was made as previously described.[37] Detailed reagents are available in the SM.

Overexpression of *myo* assay

To determine the viability of each *myo* variant when overexpressed, *UAS-myo-WT* and variant flies, as well as *UAS-empty*, were crossed to various GAL4 driving lines (*Act-GAL4*, *repo-GAL4*, *mef2-GAL4*, and *myo-T2a-GAL4*) at 18 °C, 22 °C, 25 °C, and 29 °C. Following standard practice in the fly community, two biological replicates of each cross were performed (unblinded) from each cross to determine the percentage of viable flies ($N > 150$: exact numbers are provided in Supplementary data file 1). A chi-squared test, with expected totals derived from the number of viable *GAL4 > UAS-empty* (pUAST-attB without any insert injected into VK00033) animals with the respective GAL4, was performed to determine if differences in viability were significant. No variation was estimated.

RESULTS

Patients with variants in *GDF11* exhibit multisystemic phenotypes

Probands 1–6, with both de novo and inherited variants in *GDF11* (NM_005811.4, NP_005802.1), present with complex neurological, craniofacial, skeletal, cardiovascular, connective tissue, ocular, and auditory phenotypes (Fig. 1, Table 1).[22] Of the six patients in our cohort, four have predicted nonsense or frameshift variants (p.N94Rfs*47, p.Q147Gfs*82, p.T319Nfs*5, p.Y336*), and two have missense variants (p.R295P, p.E306K) (Supplementary Table 2). One missense variant perturbs the first arginine in the RXXR motif (p.R295P) and the other missense variant reverses the charge of a conserved residue in the TGF-β domain (p.E306K) (Table 1) (Fig. 2b, c). RNA expression in PBMCs from proband 1 (p.Y336*) showed *GDF11* levels comparable to the patient's unaffected mother (Fig. 1b), suggesting that this variant does not undergo nonsense-mediated decay (NMD), which is expected as this variant lies in the final coding exon (Fig. 2c). However, quantification of GDF11 protein levels in blood plasma using ELISA showed 50% less GDF11 protein when compared to an unaffected relative (Fig. 1c). This is expected as the truncating mutant protein does not contain the antibody epitope in the TGFβ domain (Fig. 1b). The frameshift variants are not documented in gnomAD2.1.1[38] and are expected to produce a protein that lacks the functional TGF-β domain (Fig. 2b, c). Additionally, the

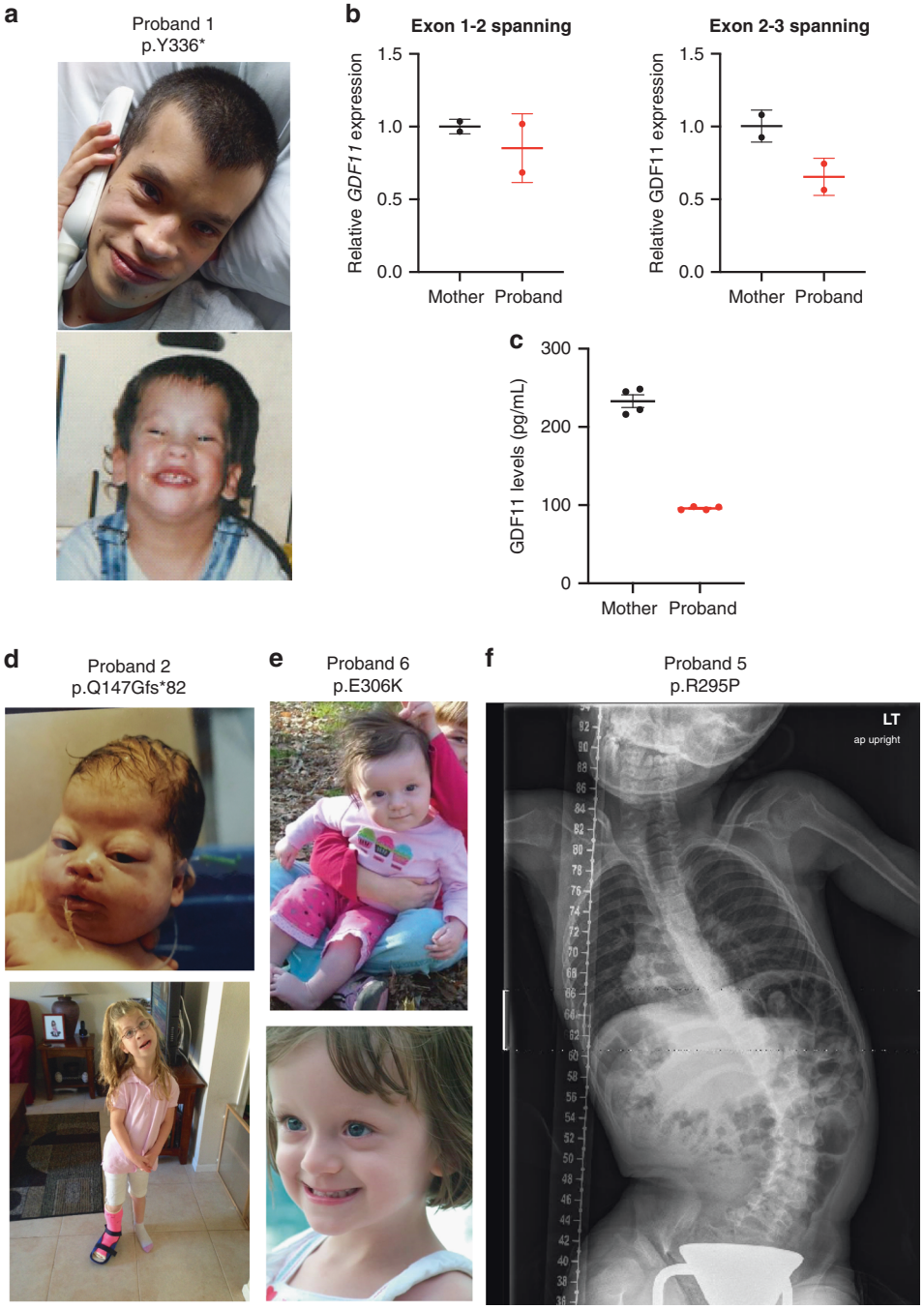

Fig. 1 Overview of patients with *GDF11* variants. (**a**) Pictures of proband 1. (**b**) *GDF11* expression was measured in peripheral blood mononuclear cells (PBMCs) derived from the proband or unaffected mother by quantitative polymerase chain reaction (qPCR) using primer sets spanning exons 1 and 2 (left) or 2 and 3 (right) normalized to *GUSB* loading control expression. RNA was collected from $n = 2$ technical replicates from $N = 1$ blood draws per patient. Error bars = SD. (**c**) GDF11 expression was measured in plasma derived from the proband or unaffected mother using a commercial GDF11 enzyme-linked immunosorbent assay (ELISA) kit (LSBio #LS-F11519) Error bars = SEM. Quantification was performed in $n = 4$ technical replicates from $N = 1$ blood draw per patient. Pictures of proband 2 (**d**) and proband 6 (**e**). X-ray of proband 5 (**f**).

probability of LOF intolerance (pLI) score for *GDF11* is 0.98 with an observed/expected (o/e) score of 0.06 in gnomAD indicating a high intolerance for LOF variants in *GDF11*.[38] A query of missense variants in *GDF11* in MARRVEL[35] revealed that p.R295P has a high CADD score[39] of 34 and is not seen in the gnomAD database (Supplementary Table 2).[38] Although the p.E306K variant is observed once in gnomAD, the variant also has a high CADD score of 27 (Supplementary Table 2). Both missense variants are predicted to be damaging by various in silico prediction algorithms.[40,41] Additionally, the missense *Z*-score for *GDF11* is 2.98, with an o/e score of 0.45, which indicates that *GDF11* is intolerant of missense variants.[38] Table 1 lists clinical presentations, which are summarized in the following paragraphs (more information is available in the Supplementary information).

Proband 1 has a de novo p.Y336* (NP_005802.1) (NM_005811.4: c.1008C>G) variant in *GDF11*. The patient was born with breathing problems, hypotonia, poor suck, and many craniofacial abnormalities including a high palate, wide nose, and a broad forehead.

Table 1. Summary of clinical information from each proband.

	Proband 1	Proband 2	Proband 3	Proband 4	Proband 5	Proband 6	
Human variant	Y336*	Q147Gfs*82	T319Nfs*5	N94Rfs*47	R295P	E306K	
Inheritance pattern	De novo	Autosomal dominant[a]	De novo	Autosomal dominant[a]	De novo	De novo	
Age of onset (y/o)	1 month	0	3	0	0	2 months	
Current age (y/o)	32	17	8	15 months	11	12	
Sex	Male	Female	Male	Male	Male	Female	
Intellectual disability	+	−	+	NA	+	−	3/5
Developmental delay	+	+	+	+	−	+	5/6
Seizures	+	−	+[b]	+	+[c]	−	4/6
Neurological abnormalities	+	+	+	+	+	+	6/6
Visual disorders	+	+	−	+	−	+	4/6
Hearing disorders	+	+	−	−	+	−	3/6
Craniofacial abnormalities	+	+	−	+	+	+	5/6
Palate abnormalities	+	+	−	−	−	+	3/6
Vertebral abnormalities	+	+	+	−	+	+	5/6
Scoliosis	+	−	−	−	+	+	3/6
Toe abnormalities	+	+	−	−	−	+	3/6
Connective tissue abnormalities	+	−	−	−	+	+	3/6
Cardiac abnormalities	+	+	−	−	+	−	3/6
Aortic dilation	+	−	−	−	+	−	2/6

Detailed reports can be found in the Supplemental materials. Proband 2 inherited the variant from her mother who has a milder phenotypic presentation.
[a]Proband 4 inherited his variant from his father, the father did not report any shared phenotypes. It is not known if the mother of proband 2 or father of proband 4 is mosaic.
[b]For proband 3 absence seizures were also reported in a sister who did not carry a variant in *GDF11*.
[c]For proband 5 seizures are likely due to Aicardi–Goutières type 6.

He displayed overlapping toes and vertebral abnormalities including a spinal fusion that led to scoliosis (Fig. 1a). He had profoundly delayed motor milestones, global developmental delay (DD), and intellectual disability (ID). Additionally, he has a dilated aortic root, macrocephaly, brain anomalies including agenesis of the corpus callosum, seizures, pronounced visual problems including congenital cataracts, bilateral central lens opacities, and myopia, and bilateral hearing loss.

Proband 2 has a maternally inherited heterozygous p.Q147Gfs*82 (NP_005802.1) (NM_005811.4:c.434_437dup) variant in *GDF11*. She presented with respiratory problems secondary to tracheomalacia at birth as well as a cleft lip and cleft palate (Fig. 1b). She has mild DD and mild bilateral hearing loss with receptive and expressive speech delays that improved greatly over time. She has craniofacial abnormalities including a large and mildly dolichocephalic head with a narrow forehead. She displays vertebral abnormalities (a long neck) and additional skeletal abnormalities with short fingers, small feet, and syndactyly of the fourth and fifth toes bilaterally. She is mildly hypotonic but otherwise normal neurologically and has no observed cardiac phenotype. The proband's mother also carries the variant and presented with similar but milder symptoms. The mother has cleft lip and palate and dolichocephaly and a long neck, missing wisdom teeth, and has narrow feet and toe abnormalities. Neurologically, the mother is normal with no ID or DD. It is not known if the mother is mosaic for the *GDF11* variant.

Proband 3 has a de novo p.T319Nfs*5 (NP_005802.1) (NM_005811.4:c.955dup) variant in *GDF11*. He has ID and DD with delayed speech and language development. Besides a pectus excavatum and mild scapula alata, he had no craniofacial or vertebral abnormalities. This individual also presented with absence seizures; however, seizures were also observed in a sister who does not have the T319Nfs*5 variant in *GDF11*.

Proband 4 has a paternally inherited heterozygous p.N94Rfs*47 (NP_005802.1) (NM_005811.4:c.279_289del) variant in *GDF11*. She presented with hypoglycemia and neonatal seizures. The individual has significant DD, microcephaly, and cerebral atrophy in addition to a lack of visual fixation. This proband has no skeletal abnormalities. The father of this proband has no reported phenotypes. It is not known if the father is mosaic for the *GDF11* variant.

Proband 5 has a de novo p.R295P (NP_005802.1) (NM_005811.4:c.884G>C) variant in *GDF11*. He has craniofacial abnormalities with marked brachycephaly and bilateral ptosis, prominent ears, and short stature with preservation of head circumference. He has additional skeletal abnormalities with marked scoliosis with hypersegmentation of his vertebrae (Fig. 1f) and has a mildly dilated aortic root. He presented with a history of regression at 18 months of age following scarlet fever with a loss of speech and language skills and delayed motor milestones. He developed spasticity, episodes of dystonia, small joint hypermobility, and contractures to hips, knees, and elbows. Prior sequencing identified a p.P193A (maternal) and a p.W1211C (paternal) variant in Adenosine deaminase RNA specific (*ADAR*) (NM_001111.4), that has been associated with a diagnosis of Aicardi–Goutières type 6 (AGS6, MIM 615010).[42–44] His seizures, dystonia, and spasticity can probably be attributed to *ADAR*; however, the remaining phenotypes have not been previously associated with AGS6.

Proband 6 has a de novo p.E306K (NP_005802.1) (NM_005811.4:c.916G>A) variant in *GDF11*. She presented with proximal weakness and myasthenic syndrome in addition to recurrent

a

Organism	Gene	DIOPT score	AA length	Alignment length	TGF-β Domain Similarity	TGF-β Domain Identity	TGF-β Domain Gaps
Mouse	Gdf11	15/16	405	407	100.0%	100.0%	0.0%
Zebrafish	gdf11	14/15	390	350	100.0%	97.0%	0.0%
Fruit Fly	myo	8/16	598	439	76.0%	46.0%	3.0%

b

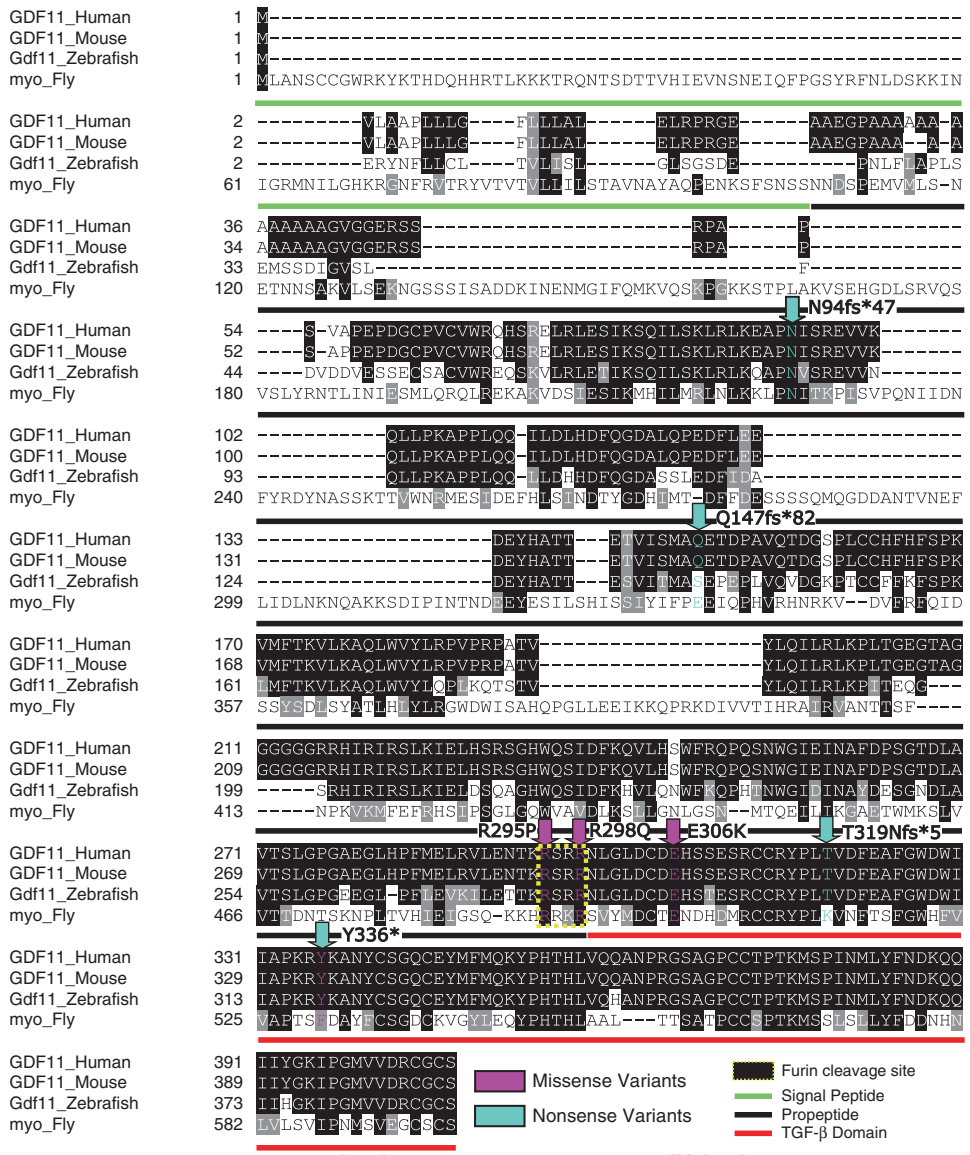

c

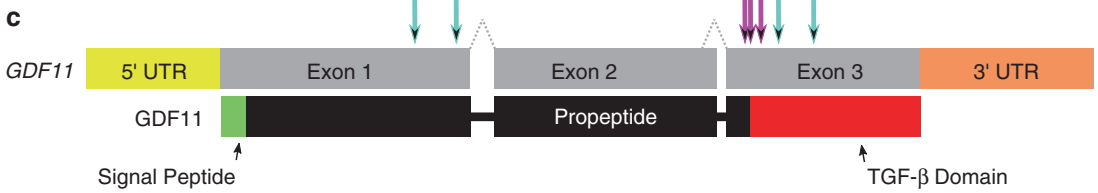

Fig. 2 *GDF11* is conserved across species. (**a**) *GDF11* is highly conserved, sharing very high DIOPT scores with mice, fish, and flies. (**b**) Both the missense variants (p.R298P and p.E306K) modeled in this study affect conserved amino acids in *Drosophila*. (**c**) Both missense variants lie within the Furin cleavage site or the TGF-β signaling domain of *GDF11* and its homologs.

retinal vasculitis (Fig. 1g) and recurrent abdominal adhesions and hepatitis with an unclear etiology. She has mild dysmorphic facial features including a slender nasal bridge with prominent columella, significant malar flattening, a prominent forehead, flat midface, and mildly high-arched palate in addition to scoliosis, pectus carinatum, spina bifida occulta, Bertalotti syndrome, and hypermobile joints. This individual has DD but no ID or cardiac abnormalities.

In summary, most patients presented with craniofacial (5/6) and vertebral (5/6) abnormalities, in agreement with previously reported phenotypes.[22] However, additional shared neurological phenotypes were present, with ID identified in 3/5 individuals, DD in 5/6, and some form of abnormal neurological presentations were identified in all probands. Other phenotypes shared among probands are visual disorders (4/6), hearing disorders (3/6), toe abnormalities (3/6), cardiac disorders (3/6) (with two individuals exhibiting aortic dilations), and connective tissue disorders (3/6). Additional individuals with copy-number variants (CNVs) in *GDF11* were identified using the DECIPHER database.[45] Of the eight patients with a CNV involving *GDF11*, three were deletions (1.28 Mb, 2.94 Mb, and 101.3 Mb) and five were duplications (2.18 Mb, 3.16 Mb, 3.42 Mb, 8.80 Mb, and 9.15 Mb). These individuals are reported to have craniofacial (4/8), vertebral (4/8), and neurological abnormalities including DD (5/8) and ID (5/8). The CNVs in the DECIPHER database include many genes neighboring *GDF11* (70 total genes in the smallest deletion [1.28 Mb] and 1,305 genes in the largest deletion [101.3 Mb]) that may influence the phenotypes in each patient. Given that GDF11 is an established key signaling protein required in the development of multiple tissues in mice,[10,11] the diverse array of phenotypes presented in this cohort and the DECIPHER database, is consistent with these observations.

gdf11 expression in zebrafish is analogous to *GDF11* expression in humans

In mice and zebrafish, the orthologs of human *GDF11* are highly conserved at the protein level (Fig. 2a). The conservation of the structure of *GDF11* across species predicts that the functions of *GDF11* may be conserved. In zebrafish, *gdf11* is expressed in numerous tissues throughout embryonic and larval development. Strong gene expression in the tailbud region at the end of gastrulation[27] is consistent with a role in posterior body axis patterning noted in avian and mammalian studies,[10,25] and expression in the brain and pharyngeal arches was noted at later larval stages.[46] Using in situ hybridization and analysis of a recently published single-cell transcriptomics data set we show that *gdf11* is expressed in organs and cell types that are affected in the probands (Supplementary results, Fig. S1, Fig. S2).

gdf11 loss-of-function in zebrafish phenocopies some patient phenotypes

Published functional analyses of *gdf11* in zebrafish are limited in scope and reported only for transient knockdown by morpholino oligonucleotide (MO) injection. In the initial analysis, *gdf11* was knocked down to evaluate the histone deacetylase regulation of liver growth.[46] In a second report, *gdf11* depletion by MO resulted in a caudal shift of *hoxc10a* expression and a corresponding caudal displacement of the pelvic fin,[27] similar to mouse mutant phenotypes.[10] To determine the role of *gdf11* in additional organ systems in fish using clean genetic tools, we used CRISPR/Cas9 gene editing to generate *gdf11* variants predicted to be LOF alleles (Fig. 3a): one allele, *b1407*, contains a truncating frameshift variant in the first exon, abrogating most of the open reading frame. The second, *b1408*, is a truncating frameshift in the third exon, removing the region that encodes the C-terminal TGF-β domain at the region similar to the truncating variant documented in proband 1. The third, *b1396*, is a 703-bp deletion removing the 5′UTR and most of the first exon to eliminate transcription and hence avoid genetic compensation.[47] Homozygotes for all three *gdf11* alleles are viable but display notable abnormalities in larval and adult stages. Alcian blue and Alizarin red staining to label cartilage and bone, respectively, in 7-dpf larval zebrafish revealed a disrupted arrangement of craniofacial elements in mutants compared to wild-type siblings (Fig. 3b–d). Mutants displayed an increased angle of articulation between the ceratohyal cartilage elements in young fish homozygous for the early and late truncating variants of 60.1 ± 4.9° and 73.3 ± 11.2°, respectively, compared to 54.4 ± 1.1° in wild-type fish ($p = 0.014$ and 0.0006). Although both are statistically significant, the defects in the later truncating *b1408* mutant were more severe and extended throughout the other cartilage elements of the jaw and face, including a morphological defect in the shape of the opercular bone (Fig. 3d). The opercular bone is one of the first ossified bone structures formed in developing fish and provides an effective model of morphogenic variations.[48,49] In 7-dpf wild-type larvae, the opercular bone had a distinctive shape, narrow medially with a fan-shaped expansion of the distal end. The wild-type opercular bone had a measured mean area of 1,950 ± 92 μm^2. By contrast, opercular bones of *gdf11*b^{1396} and *gdf11*^{1408} homozygous larvae were narrow and stick-like, lacking the distal fan, with mean areas reduced by 38% and 32% (1,207 ± 82 μm^2; $p < 0.0001$ and 1,323 ± 73.17 μm^2; $p < 0.0001$), respectively. The *gdf11*b^{1407} allele had a slightly reduced operculum (1,719 ± 62.7 μm^2), but the 12% reduction is not statistically significant ($p = 0.072$). Other signs of facial dysmorphia were apparent in animals homozygous for the *b1396* large deletion allele, where sagittal sections of the larval head revealed an abnormal rostral protrusion of the upper jaw element (Fig. 3f). This phenotype persisted in mutant adult fish (Fig. 3g, h) in which the rostral portion of the face was elongated, and the dorsoventral head width diminished relative to wild types. While we were unable to examine adult skeletal elements, measurements of live fish revealed that the body axis of young adult *b1396* homozygotes was also abnormal; the pelvic fin was posteriorized by one body segment (Fig. 3i, j), consistent both with the earlier MO study in zebrafish[27] and the mouse model in which homeotic transformations in the anterior–posterior axis were noted.[10] We conclude that zebrafish lacking *gdf11* function have several phenotypes similar to those observed in human probands.

Overexpression based assays of *GDF11* variants in *Drosophila* indicates that they are LOF variants

Variant pathogenicity prediction programs suggest that the human *GDF11* variants are damaging. To test this hypothesis, we used the fruit fly *Drosophila melanogaster*. Flies have been used effectively to identify LOF variants in human genes, elucidate mechanisms, and identify therapeutic drugs.[50] In *Drosophila*, the closest homolog to *GDF11* is *myoglianin* (*myo*) (Fig. 2a).[51] The fly *myo* gene is the only orthologue of both *GDF11* (DIOPT 7/15) and *GDF8/MSTN* (*myostatin*, DIOPT 8/15).[34] *myo* encodes a larger protein than human *GDF11* (598 vs. 405 AA), which affects protein similarity and identity scores. However, the amino acid similarity of the secreted TGF-β domain is 76%, indicating that the key signaling domain of GDF11 is highly conserved in flies (Fig. 2a). LOF alleles in *myo* have been reported to cause pupal lethality before head eversion.[33]

To determine the functionality of the probands' variants, we generated constructs containing the wild-type *myo* gene (*myo-WT*) with an upstream activation sequence (UAS). We also generated *UAS-myo* constructs with variants in the location homologous to three of the probands in this cohort, one nonsense variant p.Y336* from proband 1 (*myo-F530**), and two missense variants, p.R298P from proband 5 (*myo-R489P*) and p.E306K from proband 6 (*myo-E500K*) (Fig. S4C). We used site-directed mutagenesis and injected each construct into the VK00033 landing site via

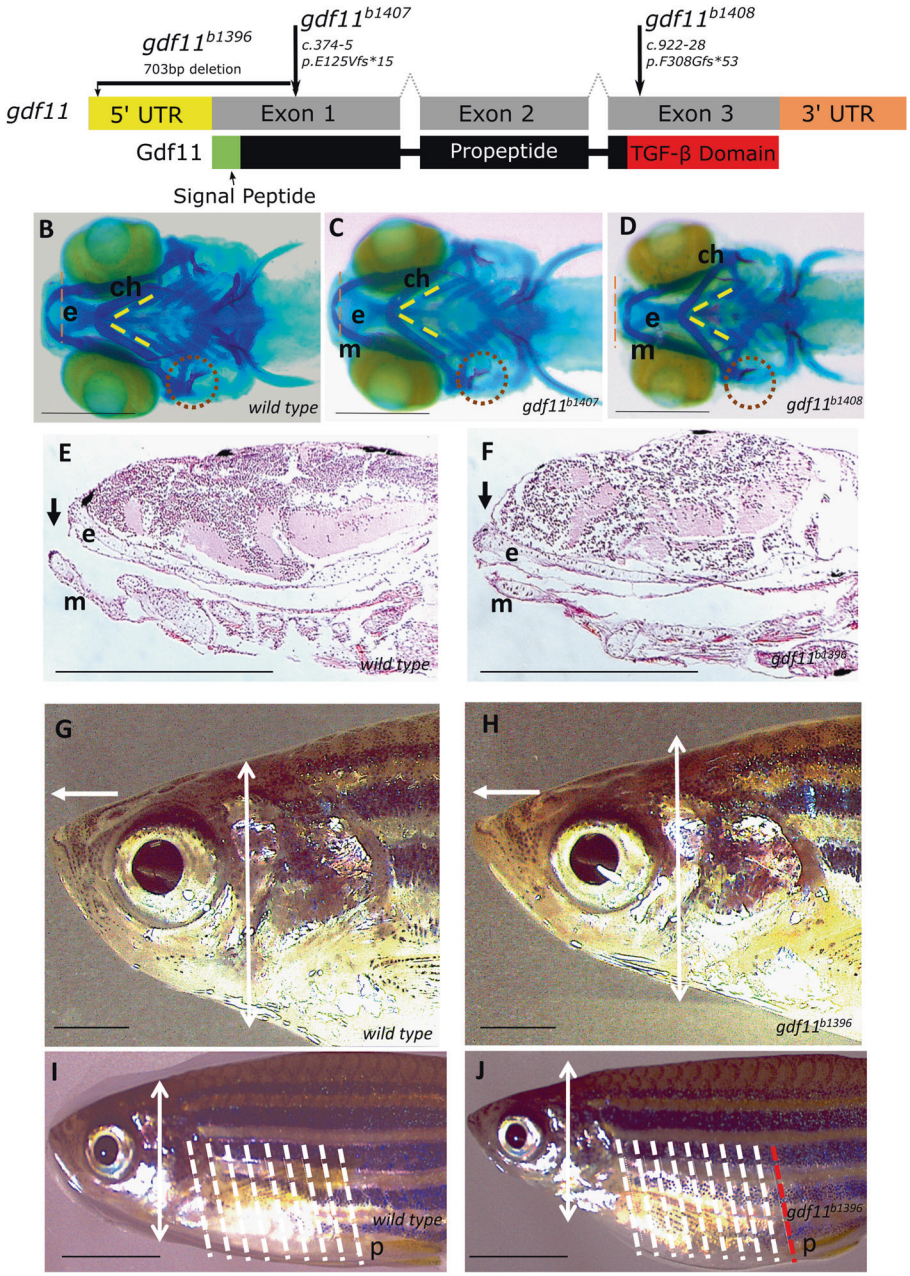

Fig. 3 Zebrafish models of gdf11 loss of function exhibit craniofacial and body axis patterning defects. (**a**) Overview of the *gdf11* mutants generated via CRISPR/Cas9 gene editing (**b**–**d**) Alcian and Alizarin staining of the 7-dpf larval head skeleton labels cartilage (blue) and bone (red) elements. From the ventral aspect, Meckel's cartilage (m) in the wild-type larval fish (**b**) extends rostrally beyond the ethmoid plate of the upper jaw (**e**, red dotted line delineates the rostral-most edge), the bilateral ceratohyal elements (ch) meet at the midline in a constrained angle of articulation (yellow dotted lines), and the opercular bone (op, red dotted circle) is ossified in with a broadening flare at its distal end. *gdf11* mutants (**c**, **d**) exhibit defects in the alignment of upper and jaw elements, in the angle of ch articulation, and the morphology of the op with a more severe phenotype observed in the late truncating allele (**d**). (**e**, **f**) Upper and lower jaw element alignment are visualized again in sagittal sections of hematoxylin and eosin (H & E) stained 7-dpf wild-type (**e**) and *gdf11* mutant (**f**) larvae, in which the ethmoid plate protrudes beyond the rostral limit of Meckel's cartilage. (**g**, **h**) Six-month *gdf11* mutant (h) rostral length measured from the anterior edge of the eye to the tip of the nose (white arrow) is 15% longer than in stage-matched wild-type (**g**; $p = 0.0007$) while the dorsoventral thickness of the head posterior to the eye (white double arrowhead, also marked in **i**,**j**) is an average of 15% less ($p = 0.001$) than in wild-type. (**i**, **j**) Regular anterior–posterior arrangements of body segments are visible on the lateral exterior or the juvenile fish (shown at 2 months in **i** and **j**), with eight such segments (white dotted lines) falling between the pectoral and pelvic (p) fins. One additional segment is noted in *gdf11* mutants (**j**, white, and red dotted lines). $N \geq 8$ for each group; scale bars: (**b**–**f**) 250 µm; (**g**–**j**) 1 mm.

phiC31 integrase mediated transgenesis to ensure constant transgene expression across constructs (Fig. S4B).[52,53] To assess the function of each *myo* variant, we first replaced the endogenous *myo* by inserting a *T2A-GAL4* CRISPR-Mediated Integration Cassette (CRIMIC) into the first coding intron of *myo*,[54] creating a *myo-T2A-GAL4* allele (Figure S4A). Unfortunately, we were not able to rescue *myo* null induced homozygous lethality (Supplemental results).

Ubiquitous overexpression of *myo* has been shown to cause pupal lethality when driven with *Actin-Gal4* (*Act-GAL4*).[33] To detect

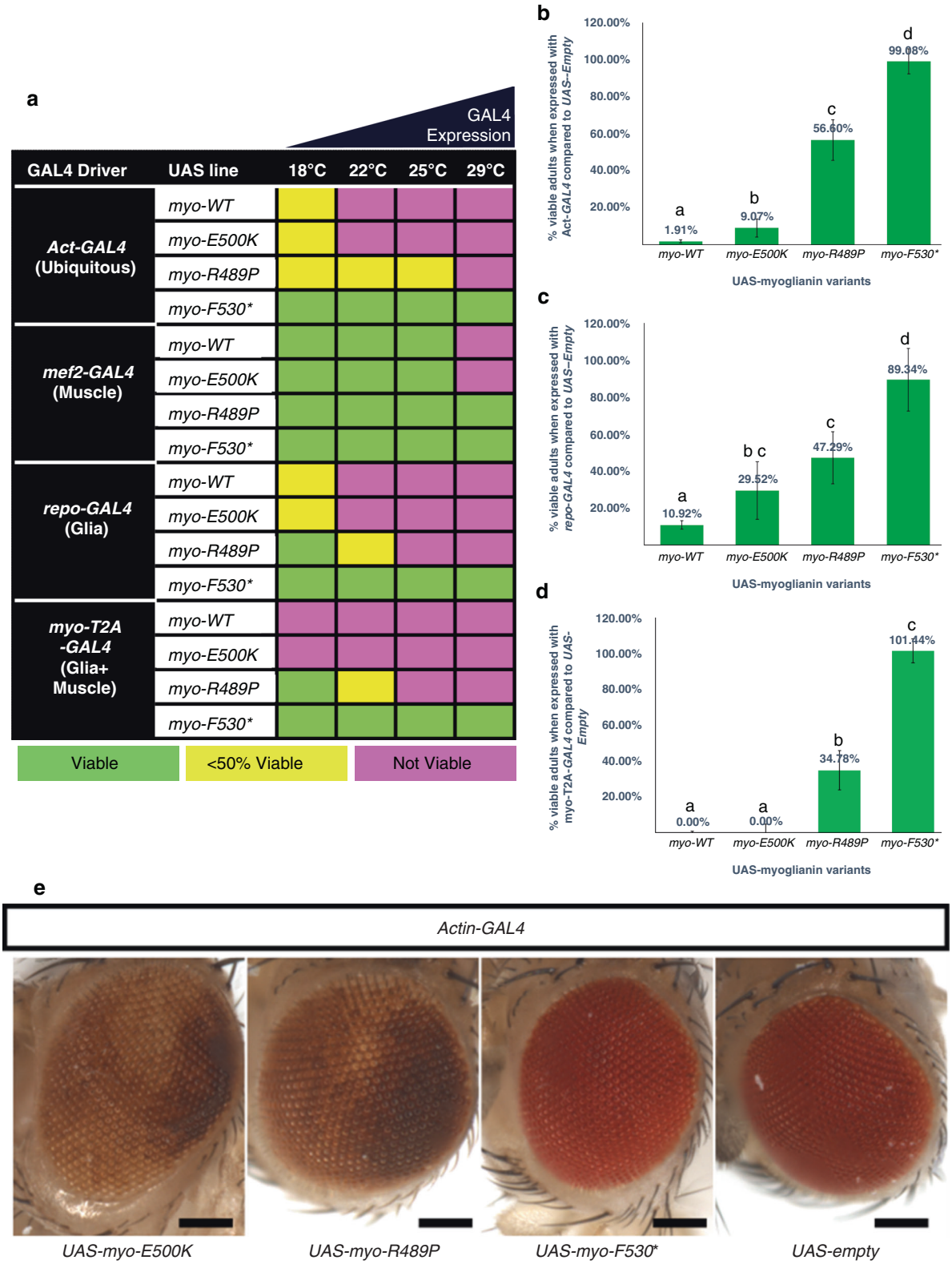

differences in functionality of the *myo* variants, we overexpress *myo-WT*, *myo-F530**, *myo-E500K*, or *myo-R489P* using *Act-GAL4* to assess the lethality of each of the variants (Fig. 4a). As a control, we use animals containing an empty UAS promoter (*UAS-empty*) inserted into the same docking site. When *UAS-myo-WT* is driven ubiquitously we observe lethality at 22 °C or higher. However ubiquitous expression of *myo* is toxic even at low levels, as only 1.91% of *Act-GAL4>UAS-myo-WT* eclose as adults compared to *Act-GAL4>UAS-empty* at 18 °C (Fig. 4b). We observe no toxicity when overexpressing *UAS-myo-F530X* with *Act-GAL4*, suggesting that this

Fig. 4 Patient variants behave as strong or mild loss-of-function alleles in flies. A mutant form of *myo* that corresponds to three of the proband's variants (p.R295P, p.E306K, and p.Y336*) along with a wild-type *myo* construct (WT) and an empty UAS-vector (negative control) were expressed with various GAL4 drivers to determine their effect when overexpressed. (**a**) Ubiquitous overexpression of *myo-WT* and overexpression with *myo-T2A-GAL4* allele is lethal except at low temperatures (18 °C) when GAL4 is less abundant. Ubiquitous overexpression of *myo-E500K* mirrors the lethality of *myo-WT*, *myo-R498P* is viable at higher temperatures and no lethality is observed when *myo-F530** is expressed at any temperature. When overexpressed specifically in muscles, *myo-WT* and *myo-E500K* are only lethal at 29 °C while *myo-R498P* and *myo-F530X* are viable. When overexpressed specifically in glial cells, the toxicity mirrors that seen with ubiquitous overexpression. The numbers of viable animals were quantified for ubiquitous expression (**b**), glial expression (**c**), and with *myo-T2A-GAL4* expression (**d**). These data indicate a decreasing scale of toxicity of *myo-WT>myo-E500K>myo-R489P > myo-F530X*. This trend is also seen with *repo-GAL4* and *myo-T2A-GAL4* at 18 °C. (**b**–**d**) Lower case letters represent groups significantly different (χ^2, $p < 0.05$) from each other. (**e**) When *myo-E500K* and *myo-R489P* variants are expressed ubiquitously at 18 °C a rough eye phenotype is observed indicating a developmental issue. All eye pictures are taken under the same magnification and were processed identically. Scale bar = 200 μm. Error bars = SD.

truncation is indeed a LOF allele. In contrast, the two missense (*p.E500K, p.R489P*) alleles do cause lethality when overexpressed, but to different degrees when compared to WT. *UAS-myo-E500K* had similar toxicity as *UAS-myo-WT* (lethal at all temperatures). However, the number of *Act-GAL4>UAS-myo-E500K* animals that eclose at 18 °C (9.00%) is significantly greater (χ^2, p value = 0.0003) than the number of *Act-GAL4>UAS-myo-WT* animals that eclose (1.91%), indicating a possible minor loss of *myo* toxicity (Fig. 4b, c). *UAS-myo-R489P* is viable at low temperatures (18 °C and 22 °C), but the viability decreased at temperatures >25 °C, suggesting the impaired function of this variant. In addition to lethality, we also find that ectopic expression of *myo* variants causes morphological phenotypes in the eye (Fig. 4e). *Act-GAL4* driving *UAS-myo-E500K* or *UAS-myo-R489P* at 18 °C causes a rough eye phenotype. This phenotype was not seen with *Act-GAL4 > UAS-myo-F530** again suggesting residual functions of the two missense variants. We did not obtain enough *UAS-myo-WT* animals to analyze whether this transgene causes a rough eye phenotype or not.

To assess the consequences of overexpression of the *myo* WT and variant alleles in the cells where *myo* is normally expressed we used *myo-T2A-GAL4* (muscle and glia), *mef2-GAL4* (muscle), and *repo-GAL4* (glia) to drive various *myo* transgenes at different temperatures. The same trend for toxicity was seen for each driver with *UAS-myo-WT* showing the strongest toxicity, followed by *UAS-myo-E500K* then *UAS-myo-R489P*, and finally *UAS-myo-F530** and *UAS-empty* causing no lethality (Supplementary results, Fig. 4a–d). The absence of increased lethality at any temperature when the *myo-F530** allele is expressed with any GAL4 driver indicates that the allele is unlikely to have a dominant negative effect. These data indicate that *myo-F530** is a strong LOF allele, *myo-R489P* a partial LOF allele, and *myo-E500K* a milder LOF allele.

DISCUSSION

Craniofacial and vertebral abnormalities are related to LOF variants in *GDF11* in human patients[22] and rodent knockout models.[10] Here, we report four patients with strong LOF variants in *GDF11*, with only one patient having severe craniofacial and vertebrae abnormalities. Patients with truncation alleles in *GDF11* present with a higher prevalence of neurological abnormalities, developmental delays, and visual problems. Additionally, neurological, developmental, and ocular abnormalities have a stronger correlation with the degree of *GDF11* LOF than do vertebral and craniofacial abnormalities, indicating *GDF11* dosage may have a greater influence on nervous system development than on the development of other tissues.

In zebrafish, craniofacial abnormalities vary in severity among LOF alleles. Variants that result in NMD have been found to trigger genetic compensation through the activation of related genes.[47] Thus, the milder phenotype observed in the early truncating allele (*b1407*) may be due to this transcriptional switch, whereas the later truncation (*b1408*), would be presumed to escape genetic compensation. The large deletion (*b1396*), which was designed to block transcription altogether, is predicted to be immune from genetic compensation and thus a complete LOF. The viability and somewhat milder phenotypes of these zebrafish mutant alleles, compared to the mouse and fly models, suggest some functional redundancy, which may mirror some of the clinical phenotypes of the probands in this study.

Interestingly, the severity of the LOF alleles reported from the fly experiments correlates with the severity of the neurological phenotypes seen in our patient cohort. The four probands with nonsense variants all show profound DD and 3/4 probands have associated ID. The patient with a partial LOF allele (proband 5—p.R295P) presents with ID but not DD, a milder presentation than the complete LOF variant patients but more severe than the milder LOF patient (proband 6—p.E306K). This gradient of symptom severity indicates that the degree of *GDF11* function loss in patients reflects the severity of the neurological disorder. In agreement with this observation, LOF alleles in *Drosophila myo*[33] and mice *Gdf11*[10] have severe nervous system defects. Additionally, overexpression of *myo* variants causes a rough eye phenotype in *Drosophila*, indicative of a neurodevelopmental defect in the fly visual system. Although the severity of craniofacial and vertebral dysmorphism in probands is variable, genotype–phenotype correlation can be seen in these organ systems. Probands with full cleft lip/palate have a complete LOF nonsense variant and those with minor craniofacial phenotypes have partial/milder LOF alleles. However, the minor phenotypic presentation in the mother of proband 2 and the lack of any reported phenotypes in the father of proband 4 is an indicator of the variable expressivity and incomplete penetrance associated with *GDF11* LOF variants. In agreement with this is the lack of vertebral phenotypes in probands 3 and 4, the lack of craniofacial dysmorphism in proband 3 and the variability of phenotypes in a previously reported family with a *GDF11* variant.[22] These phenotypes are likely more influenced by other genetic or environmental factors than the neurological phenotypes, which more closely correlate with the severity of the *GDF11* LOF variants.

How loss of *GDF11* disrupts neuronal development is unclear. In mouse olfactory epithelium, Gdf11 negatively regulates neurogenesis by promoting cell cycle arrest in neuronal progenitors via 27^{Kip1} and/or $p21c^{ip1}$ and inactivation of Foxg1.[23,55] Also in the brain, Gdf11 acts as a negative regulator of gliogenesis, favoring stem cell differentiation into neuronal precursor cells.[56] In contrast, in the spinal cord, loss of Gdf11 causes a decrease in proliferation of spinal cord motoneurons in addition to aberrant rostral/caudal patterning of motoneurons as a result of expanded *Hoxc* expression.[25,29] In the retina, Gdf11 is a negative regulator of retinal ganglion cell proliferation. Interestingly the latter is not via cell cycle arrest as in the olfactory epithelium, but instead via downregulation of *Math5*.[26] Hence, although *Gdf11* is a key player in neuronal development, predicting how these disruptions manifest in a phenotype in humans is not yet obvious.

The impact on the cardiovascular system is also seen in patients with *GDF11* LOF variants. *GDF11* is expressed in cardiac muscle in

adults and is expressed in neural crest cells that signal the development of cardiac structures such as the aorta in mammals and zebrafish. In both adult mice and humans, the role of *GDF11* is controversial with debate on whether increasing circulating GDF11 helps cardiac health,[20,57–59] and the role of *GDF11* in the developing heart has not been well studied in vivo in model organisms. Cardiomyocyte *Gdf11* knockout mice have left ventricular dilation,[60] indicating a potential association between a loss of *GDF11* and cardiovascular abnormalities, which is consistent with the two patients in our cohort with aortic dilation. Gdf11 initiates intracellular Smad2 activation by binding to the Activin receptors TGFBR1 and ACVR2B.[12–14] LOF variants in human *TGFBR1* and *ACVR2B* are associated with defects in cardiac development.[61,62] Among our cohort of patients with *GDF11* LOF variants, 3/6 patients have cardiac abnormalities and two have aortic dilations. The influence of GDF11 specifically on the developing human heart is likely to be complex due to the compensatory roles of MSTN and its ability to bind the same receptors as GDF11.[63] The expression of these different GDF paralogs, the diversity of the receptors, and modulators, such as follistatin, may impact how cardiac malformations present in *GDF11* LOF variants. However, cardiac abnormalities, particularly aortic dilations, should be screened for in patients with variants in *GDF11*.

Both partial LOF variants present in this cohort, in addition to a family member in the previously reported family,[22] present with connective tissue abnormalities resulting in hypermobile joints. Because the most common cause of joint hypermobility is a lack of collagen and GDF11 induces the expression of collagen I and III, the connective tissue disorders are seen in patients may also be due to partial LOF variants in *GDF11*,[64] which will require further biological studies.

In conclusion, we have identified a cohort of six patients from six families with LOF variants in *GDF11*. The cohort has complex clinical presentations significantly expanding the phenotypes linked to variants in this gene. We have generated *gdf11* zebrafish mutants that exhibit craniofacial and body axis patterning abnormalities that reflect *gdf11* expression patterns and some of the key clinical presentations of the human subjects. Using *Drosophila*, we have been able to determine the degree of *GDF11* functional loss for a subset of variants, showing that LOF severity measured in flies correlates with the severity of neurological phenotypes in humans. The variable expressivity of *GDF11*-associated phenotypes is likely a result of the complexities and redundancies of GDF signaling throughout development as well as other genetic and environmental factors. To further elucidate these additional factors, we will need an expanded cohort of patients with LOF variants in *GDF11*. This study provides the resources for modeling and evaluating *GDF11* LOF variants in model organisms and the potential phenotypes caused by *GDF11* variants.

DATA AND CODE AVAILABILITY

The paper includes all data sets/code generated or analyzed during this study.

Received: 25 January 2021; Revised: 4 May 2021; Accepted: 5 May 2021;
Published online: 10 June 2021

REFERENCES

1. Lee, S. J. Identification of a novel member (GDF-1) of the transforming growth factor-β superfamily. *Mol. Endocrinol.* **4**, 1034–1040 (1990).
2. Akhurst, R. J. & Hata, A. Targeting the TGFβ signalling pathway in disease. *Nat. Rev. Drug Discov.* **11**, 790–811 (2012).
3. Frikha, R. Klippel-Feil syndrome: a review of the literature. *Clin. Dysmorphol.* **29**, 35–37 (2020).
4. Naikmasur, V. G., Sattur, A. P., Kirty, R. N. & Thakur, A. R. Type III Klippel-Feil syndrome: case report and review of associated craniofacial anomalies. *Odontology* **99**, 197–202 (2011).
5. Asai-Coakwell, M. et al. Incomplete penetrance and phenotypic variability characterize Gdf6-attributable oculo-skeletal phenotypes. *Hum. Mol. Genet.* **18**, 1110–1121 (2009).
6. Otsuka, F., McTavish, K. J. & Shimasaki, S. Integral role of GDF-9 and BMP-15 in ovarian function. *Mol. Reprod. Dev.* **78**, 9–21 (2011).
7. McPherron, A. C., Huynh, T. V. & Lee, S. J. Redundancy of myostatin and growth/differentiation factor 11 function. *BMC Dev. Biol.* **9**, 24 (2009).
8. Bandyopadhyay, A. et al. Genetic analysis of the roles of BMP2, BMP4, and BMP7 in limb patterning and skeletogenesis. *PLoS Genet.* **2**, 2116–2130 (2006).
9. Zhao, R., Lawler, A. M. & Lee, S. J. Characterization of GDF-10 expression patterns and null mice. *Dev. Biol.* **212**, 68–79 (1999).
10. McPherron, A. C., Lawler, A. M. & Lee, S. J. Regulation of anterior/posterior patterning of the axial skeleton by growth/differentiation factor 11. *Nat. Genet.* **22**, 260–264 (1999).
11. Walker, R. G. et al. Biochemistry and biology of GDF11 and myostatin: similarities, differences and questions for future investigation HHS Public Access. *Circ Res* **118**, 1125–1142 (2016).
12. Paul, Oh,S. et al. Activin type IIA and IIB receptors mediate Gdf11 signaling in axial vertebral patterning. *Genes Dev.* **16**, 2749–2754 (2002).
13. Rebbapragada, A., Benchabane, H., Wrana, J. L., Celeste, A. J. & Attisano, L. Myostatin signals through a transforming growth factor β-like signaling pathway to block adipogenesis. *Mol. Cell. Biol.* **23**, 7230–7242 (2003).
14. Andersson, O., Reissmann, E., Jörnvall, H. & Ibáñez, C. F. Synergistic interaction between Gdf1 and Nodal during anterior axis development. *Dev. Biol.* **293**, 370–381 (2006).
15. Bajikar, S. S. et al. Tumor-suppressor inactivation of GDF11 occurs by precursor sequestration in triple-negative breast cancer. *Dev. Cell* **43**, 418–435. e13 (2017).
16. C. McPherron, A. Metabolic functions of myostatin and GDF11. *Immunol. Endocr. Metab. Agents Med. Chem.* **10**, 217–231 (2012).
17. Gamer, L. W. et al. A novel BMP expressed in developing mouse limb, spinal cord, and tail bud is a potent mesoderm inducer in Xenopus embryos. *Dev. Biol.* **208**, 222–232 (1999).
18. Nakashima, M., Toyono, T., Akamine, A. & Joyner, A. Expression of growth/differentiation factor 11, a new member of the BMP/TGFβ superfamily during mouse embryogenesis. *Mech. Dev.* **80**, 185–189 (1999).
19. Zhang, Y. et al. Growth differentiation factor 11 is a protective factor for osteoblastogenesis by targeting PPARgamma. *Gene.* **557**, 209–214 (2015).
20. Loffredo, F. S. et al. Growth differentiation factor 11 is a circulating factor that reverses age-related cardiac hypertrophy. *Cell.* **153**, 828–839 (2013).
21. Jeanplong, F. et al. Growth and differentiation factor-11 is developmentally regulated in skeletal muscle and inhibits myoblast differentiation. *Open J. Mol. Integr. Physiol.* **2**, 127–138 (2012).
22. Cox, T. C. et al. Mutations in GDF11 and the extracellular antagonist, Follistatin, as a likely cause of Mendelian forms of orofacial clefting in humans. *Hum. Mutat.* **40**, 1813–1825 (2019).
23. Wu, H. H. et al. Autoregulation of neurogenesis by GDF11. *Neuron*. **37**, 197–207 (2003).
24. Suh, J. et al. GDF11 promotes osteogenesis as opposed to MSTN, and follistatin, a MSTN/GDF11 inhibitor, increases muscle mass but weakens bone. *Proc. Natl. Acad. Sci. U. S. A.* **117**, 4910–4920 (2020).
25. Liu, J. P. The function of growth/differentiation factor 11 (Gdf11) in rostrocaudal patterning of the developing spinal cord. *Development*. **133**, 2865–2874 (2006).
26. Kim, J. et al. Developmental biology: GDF11 controls the timing of progenitor cell competence in developing retina. *Science (80-.).* **308**, 1927–1930 (2005).
27. Murata, Y. et al. Allometric growth of the trunk leads to the rostral shift of the pelvic fin in teleost fishes. *Dev. Biol.* **347**, 236–245 (2010).
28. Goldstein, J. M., et al. Variation in zygotic CRISPR/Cas9 gene editing outcomes generates novel reporter and deletion alleles at the Gdf11 locus. *Sci. Rep.* **9**, 18613 (2019).
29. Shi, Y. & Liu, J. P. Gdf11 facilitates temporal progression of neurogenesis in the developing spinal cord. *J. Neurosci.* **31**, 883–893 (2011).
30. Rodríguez-Marí, A. et al. Characterization and expression pattern of zebrafish anti-Müllerian hormone (amh) relative to sox9a, sox9b, and cyp19a1a, during gonad development. *Gene Expr. Patterns* **5**, 655–667 (2005).
31. Farnsworth, D. R., Saunders, L. M. & Miller, A. C. A single-cell transcriptome atlas for zebrafish development. *Dev. Biol.* **459**, 100–108 (2020).
32. Walker, M. B. & Kimmel, C. B. A two-color acid-free cartilage and bone stain for zebrafish larvae. *Biotech. Histochem.* **82**, 23–28 (2007).
33. Awasaki, T., Huang, Y., O'Connor, M. B. & Lee, T. Glia instruct developmental neuronal remodeling through TGF-Î 2 signaling. *Nat. Neurosci.* **14**, 821–823 (2011).

34. Hu, Y. et al. An integrative approach to ortholog prediction for disease-focused and other functional studies. *BMC Bioinformatics.* **12**, 357 (2011).
35. Wang, J. et al. MARRVEL: integration of human and model organism genetic resources to facilitate functional annotation of the human genome. *Am. J. Hum. Genet.* **100**, 843–853 (2017).
36. Chung, Hlok et al. Loss- or gain-of-function mutations in ACOX1 cause axonal loss via different mechanisms. *Neuron* **106**, 589–606.e6 (2020).
37. Kanca, O., et al. An efficient CRISPR-based strategy to insert small and large fragments of DNA using short homology arms. *Elife*. **8**, e51539 (2019).
38. Karczewski, K. J. et al. The mutational constraint spectrum quantified from variation in 141,456 humans. *Nature.* **581**, 434–443 (2020).
39. Rentzsch, P., Witten, D., Cooper, G. M., Shendure, J. & Kircher, M. CADD: predicting the deleteriousness of variants throughout the human genome. *Nucleic Acids Res.* **47**, D886–D894 (2019).
40. Yang, H. & Wang, K. Genomic variant annotation and prioritization with ANNOVAR and wANNOVAR. *Nat. Protoc.* **10**, 1556–1566 (2015).
41. Adzhubei, I. A. et al. A method and server for predicting damaging missense mutations. *Nat. Methods.* **7**, 248–249 (2010).
42. Crow, Y. J. et al. Mutations in ADAR1, IFIH1, and RNASEH2B presenting as spastic paraplegia. *Neuropediatrics*. **45**, 386–391 (2014).
43. Livingston, J. H. et al. A type I interferon signature identifies bilateral striatal necrosis due to mutations in ADAR1. *J. Med. Genet.* **51**, 76–82 (2014).
44. Rice, G. I. et al. Mutations in ADAR1 cause Aicardi-Goutières syndrome associated with a type i interferon signature. *Nat. Genet.* **44**, 1243–1248 (2012).
45. Firth, H. V. et al. DECIPHER: Database of Chromosomal Imbalance and Phenotype in Humans Using Ensembl Resources. *Am. J. Hum. Genet.* **84**, 524–533 (2009).
46. Farooq, M. et al. Histone deacetylase 3 (hdac3) is specifically required for liver development in zebrafish. *Dev. Biol.* **317**, 336–353 (2008).
47. El-Brolosy, M. A. et al. Genetic compensation triggered by mutant mRNA degradation. *Nature.* **568**, 193–197 (2019).
48. Huycke, T. R., Frank Eames, B. & Kimmel, C. B. Hedgehog-dependent proliferation drives modular growth during morphogenesis of a dermal bone. *Development.* **139**, 2371–2380 (2012).
49. Tarasco, M., Laizé, V., Cardeira, J., Cancela, M. L. & Gavaia, P. J. The zebrafish operculum: a powerful system to assess osteogenic bioactivities of molecules with pharmacological and toxicological relevance. *Comp. Biochem. Physiol. C Toxicol. Pharmacol.* **197**, 45–52 (2017).
50. Bellen, H. J., Wangler, M. F. & Yamamoto, S. The fruit fly at the interface of diagnosis and pathogenic mechanisms of rare and common human diseases. *Hum. Mol. Genet.* **28**, R207–R214 (2019).
51. Lo, P. C. H. & Frasch, M. Sequence and expression of myoglianin, a novel Drosophila gene of the TGF-β superfamily. *Mech. Dev.* **86**, 171–175 (1999).
52. Groth, A. C., Fish, M., Nusse, R. & Calos, M. P. Construction of transgenic Drosophila by using the site-specific integrase from phage φC31. *Genetics* **166**, 1775–1782 (2004).
53. Venken, K. J. T., He, Y., Hoskins, R. A. & Bellen, H. J. P[acman]: a BAC transgenic platform for targeted insertion of large DNA fragments in D. melanogaster. *Science (80-.).* **314**, 1747–1751 (2006).
54. Lee, P. T. et al. A gene-specific T2a-GAL4 library for drosophila. *Elife*. **7**, e35574 (2018).
55. Kawauchi, S. et al. Foxg1 promotes olfactory neurogenesis by antagonizing Gdf11. *Development*. **136**, 1453–1464 (2009).
56. Gokoffski, K. K. et al. Activin and GDF11 collaborate in feedback control of neuroepithelial stem cell proliferation and fate. *Development.* **138**, 4131–4142 (2011).
57. Schafer, M. J. et al. Quantification of GDF11 and myostatin in human aging and cardiovascular disease. *Cell Metab.* **23**, 1207–1215 (2016).
58. Smith, S. C. et al. GDF11 does not rescue aging-related pathological hypertrophy. *Circ. Res.* **117**, 926–932 (2015).
59. Olson, K. A. et al. Association of growth differentiation factor 11/8, putative anti-ageing factor, with cardiovascular outcomes and overall mortality in humans: analysis of the Heart and Soul and HUNT3 cohorts. *Eur. Heart J.* **36**, 3426–3434 (2015).
60. Garbern, J. et al. Analysis of Cre-mediated genetic deletion of Gdf11 in cardiomyocytes of young mice. *Am. J. Physiol. Heart Circ. Physiol.* **317**, H201–H212. (2019).
61. Loeys, B. L. et al. A syndrome of altered cardiovascular, craniofacial, neurocognitive and skeletal development caused by mutations in TGFBR1 or TGFBR2. *Nat. Genet.* **37**, 275–281 (2005).
62. Kosaki, R. et al. Left-right axis malformations associated with mutations in ACVR2B, the gene for human activin receptor type IIB. *Am. J. Med. Genet.* **82**, 70–76 (1999).
63. Egerman, M. A. et al. GDF11 increases with age and inhibits skeletal muscle regeneration. *Cell Metab.* **22**, 164–174 (2015).
64. Tito, A. et al. The growth differentiation factor 11 is involved in skin fibroblast ageing and is induced by a preparation of peptides and sugars derived from plant cell cultures. *Mol. Biotechnol.* **61**, 209–220 (2019).

ACKNOWLEDGEMENTS

We thank the patients and their families who participated in this study. The research reported in this paper was supported by the National Institutes of Health (NIH_ Common Fund, the Office of Strategic Coordination and Office of the NIH Director under award numbers U01HG007942 (BCM sequencing core), U54NS093793 (Model Organism Screening Center of the Undiagnosed Diseases Network), R24OD026591 (J.H.P and M.W), and U01HG007690 (BWH clinical site). The Care4Rare Research Consortium performed the reanalysis of the exome data for patient 5 and is funded by Genome Canada and the Ontario Genomics Institute (OGI-147), the Canadian Institutes of Health Research, Ontario Research Fund, Genome Alberta, Genome British Columbia, Genome Q8 Quebec, and Children's Hospital of Eastern Ontario Foundation. H.J.B. and S.Y. are supported by R24OD022005 from the Office of Research Infrastructure Programs (ORIP) at NIH. *myo-T2A-GAL4* generation was funded as part of the genome disruption project (NIGMS GM132087). The content is solely the responsibility of the authors and does not necessarily represent the official views of the NIH. T.A.R. has been supported by The Cullen Foundation. S.S.B. is supported by F32HD100048 from the Eunice Kennedy Shriver National Institute of Child Health and Human Development (NICHD) at NIH. H.J.B. is an investigator of the Howard Hughes Medical Institute.

AUTHOR CONTRIBUTIONS

Conceptualization: T.A.R, J.B.P., E.F., S.S.B., U.D.N., J.H.P., M.F.W., S.Y., J.K., M.W., H.J.B. Data curation: T.A.R., J.B.P., J.A.R., J.Z., O.K., P.J.B, E.S.C., V.S., K.P., R.A.J., C.K., M.O., T.L., S.R., D.D., J.S.C.C., S.L., J.M.S., J.K. Formal analysis: T.A.R., J.B.P., S.S.B; Funding acquisition: T.A.R., S.S.B., U.D.N., J.H.P., M.F.W., S.Y., J.K., M.W., H.J.B., D.D. Investigation: T.A.R, J.B.P., S.S.B., J.P., A.A.L., E.J.F., Y.L.Y., J.Z. Resources: T.A.R., J.B.P, E.F., S.S.B, J.Z, O.K. Supervision: T.A.R, J.B.P; Visualization: T.A.R, J.B.P. Writing—original draft: T.A.R. Writing—review & editing: T.A.R, J.B.P., E.F., S.S.B., A.A.L, J.A.R, J.Z., O.K., P.J.B., V.S., D.D., J.S.C.C., J.H.P., S.Y., J.K., M.W., H.J.B.

ETHICS DECLARATION

Written informed consent for genetic testing and publication of relevant findings and photographs was obtained from all patients or their parents. Research using patient cells is approved by the Institutional Review Board for Human Subject Research for Baylor College of Medicine and Affiliated Hospitals (BCM IRB) for translational models of neurological disease at the neurological research institute (Human Subjects Assurance Number: 00000286). The BCM IRB is organized, operates, and is registered with the United States Office for Human Research Protections according to the regulations codified in the United States Code of Federal Regulations at 45 CFR 46 and 21 CFR 56. The BCM IRB operates under the BCM Federal Wide Assurance Number 00000286, as well as those of hospitals and institutions affiliated with the College. Zebrafish were raised and all experiments were conducted according to standard protocols approved by the University of Oregon Institutional Animal Care and Use Committee (IACUC).

COMPETING INTERESTS

The Department of Molecular and Human Genetics at Baylor College of Medicine receives revenue from clinical genetic testing conducted at Baylor Genetics Laboratories. The other authors declare no competing interests.

ADDITIONAL INFORMATION

Supplementary information The online version contains supplementary material available at https://doi.org/10.1038/s41436-021-01216-8.

Correspondence and requests for materials should be addressed to H.J.B.

Reprints and permission information is available at http://www.nature.com/reprints

Publisher's note Springer Nature remains neutral with regard to jurisdictional claims in published maps and institutional affiliations.

UNDIAGNOSED DISEASES NETWORK

Maria T. Acosta[14], Margaret Adam[15], David R. Adams[14], Pankaj B. Agrawal[16], Mercedes E. Alejandro[17], Justin Alvey[18], Laura Amendola[15], Ashley Andrews[18], Euan A. Ashley[19], Mahshid S. Azamian[17], Carlos A. Bacino[17], Guney Bademci[20], Eva Baker[14], Ashok Balasubramanya[17], Dustin Baldridge[21], Jim Bale[18], Michael Bamshad[15], Deborah Barbouth[20], Pinar Bayrak-Toydemir[18], Anita Beck[15], Alan H. Beggs[16], Edward Behrens[22], Gill Bejerano[19], Jimmy Bennet[15], Beverly Berg-Rood[15], Jonathan A. Bernstein[19], Gerard T. Berry[16], Anna Bican[23], Stephanie Bivona[20], Elizabeth Blue[15], John Bohnsack[18], Carsten Bonnenmann[14], Devon Bonner[19], Lorenzo Botto[18], Brenna Boyd[15], Lauren C. Briere[16], Elly Brokamp[23], Gabrielle Brown[24], Elizabeth A. Burke[14], Lindsay C. Burrage[17], Manish J. Butte[24], Peter Byers[15], William E. Byrd[25], John Carey[18], Olveen Carrasquillo[20], Ta Chen Peter Chang[20], Sirisak Chanprasert[15], Hsiao-Tuan Chao[17], Gary D. Clark[17], Terra R. Coakley[26], Laurel A. Cobban[16], Joy D. Cogan[23], Matthew Coggins[16], F. Sessions Cole[27], Heather A. Colley[14], Cynthia M. Cooper[16], Heidi Cope[28], William J. Craigen[17], Andrew B. Crouse[25], Michael Cunningham[15], Precilla D'Souza[14], Hongzheng Dai[17], Surendra Dasari[29], Joie Davis[14], Jyoti G. Dayal[14], Matthew Deardorff[22], Esteban C. Dell'Angelica[24], Shweta U. Dhar[17], Katrina Dipple[15], Daniel Doherty[15], Naghmeh Dorrani[24], Argenia L. Doss[14], Emilie D. Douine[24], David D. Draper[14], Laura Duncan[23], Dawn Earl[15], David J. Eckstein[14], Lisa T. Emrick[17], Christine M. Eng[30], Cecilia Esteves[31], Marni Falk[22], Liliana Fernandez[26], Carlos Ferreira[14], Elizabeth L. Fieg[16], Laurie C. Findley[14], Paul G. Fisher[26], Brent L. Fogel[24], Irman Forghani[20], Laure Fresard[26], William A. Gahl[14], Ian Glass[15], Bernadette Gochuico[14], Rena A. Godfrey[14], Katie Golden-Grant[15], Alica M. Goldman[17], Madison P. Goldrich[14], David B. Goldstein[32], Alana Grajewski[20], Catherine A. Groden[14], Irma Gutierrez[24], Sihoun Hahn[15], Rizwan Hamid[23], Neil A. Hanchard[17], Kelly Hassey[22], Nichole Hayes[27], Frances High[16], Anne Hing[15], Fuki M. Hisama[15], Ingrid A. Holm[16], Jason Hom[26], Martha Horike-Pyne[15], Alden Huang[24], Yong Huang[26], Laryssa Huryn[14], Rosario Isasi[20], Fariha Jamal[17], Gail P. Jarvik[15], Jeffrey Jarvik[15], Suman Jayadev[15], Lefkothea Karaviti[17], Jennifer Kennedy[23], Dana Kiley[27], Isaac S. Kohane[31], Jennefer N. Kohler[26], Deborah Krakow[24], Donna M. Krasnewich[14], Elijah Kravets[26], Susan Korrick[16], Mary Koziura[23], Joel B. Krier[16], Seema R. Lalani[17], Byron Lam[20], Christina Lam[15], Grace L. LaMoure[14], Brendan C. Lanpher[29], Ian R. Lanza[29], Lea Latham[14], Kimberly LeBlanc[31], Brendan H. Lee[17], Hane Lee[24], Roy Levitt[20], Richard A. Lewis[17], Sharyn A. Lincoln[16], Pengfei Liu[30], Xue Zhong Liu[20], Nicola Longo[18], Sandra K. Loo[24], Joseph Loscalzo[16], Richard L. Maas[16], John MacDowall[14], Ellen F. Macnamara[14], Calum A. MacRae[16], Valerie V. Maduro[14], Marta M. Majcherska[26], Bryan C. Mak[24], May Christine V. Malicdan[14], Laura A. Mamounas[14], Teri A. Manolio[14], Rong Mao[18], Kenneth Maravilla[15], Thomas C. Markello[14], Ronit Marom[17], Gabor Marth[18], Beth A. Martin[26], Martin G. Martin[24], Julian A. Martínez-Agosto[24], Shruti Marwaha[26], Jacob McCauley[20], Allyn McConkie-Rosell[28], Colleen E. McCormack[26], Alexa T. McCray[31], Elisabeth McGee[24], Heather Mefford[15], J. Lawrence Merritt[15], Matthew Might[25], Ghayda Mirzaa[15], Eva Morava[29], Paolo Moretti[18], Paolo M. Moretti[17], Deborah Mosbrook-Davis[14], John J. Mulvihill[14], David R. Murdock[17], Anna Nagy[31], Mariko Nakano-Okuno[25], Avi Nath[14], Stan F. Nelson[24], John H. Newman[23], Sarah K. Nicholas[17], Deborah Nickerson[15], Shirley Nieves-Rodriguez[24], Donna Novacic[14], Devin Oglesbee[29], James P. Orengo[17], Laura Pace[18], Stephen Pak[33], J. Carl Pallais[16], Christina GS. Palmer[24], Jeanette C. Papp[24], Neil H. Parker[24], John A. Phillips III[23], Jennifer E. Posey[17], Lorraine Potocki[17], Bradley Power[14], Barbara N. Pusey[14], Aaron Quinlan[18], Wendy Raskind[15], Archana N. Raja[26], Deepak A. Rao[16], Genecee Renteria[24], Chloe M. Reuter[26], Lynette Rives[23], Amy K. Robertson[23], Lance H. Rodan[16], Jill A. Rosenfeld[17], Natalie Rosenwasser[15], Francis Rossignol[14], Maura Ruzhnikov[26], Ralph Sacco[20], Jacinda B. Sampson[26], Susan L. Samson[17], Mario Saporta[20], C. Ron Scott[14], Judy Schaechter[20], Timothy Schedl[33], Kelly Schoch[28], Daryl A. Scott[17], Vandana Shashi[28], Jimann Shin[33], Rebecca Signer[24], Edwin K. Silverman[16], Janet S. Sinsheimer[24], Kathy Sisco[27], Edward C. Smith[28], Kevin S. Smith[26], Emily Solem[23], Lilianna Solnica-Krezel[33], Ben Solomon[14], Rebecca C. Spillmann[28], Joan M. Stoler[16], Jennifer A. Sullivan[28], Kathleen Sullivan[22], Angela Sun[15], Shirley Sutton[26], David A. Sweetser[16], Virginia Sybert[15], Holly K. Tabor[26], Amelia L. M. Tan[31], Queenie K.-G. Tan[28], Mustafa Tekin[20], Fred Telischi[20], Willa Thorson[20], Audrey Thurm[14], Cynthia J. Tifft[14], Camilo Toro[14], Alyssa A. Tran[17], Brianna M. Tucker[26], Tiina K. Urv[14], Adeline Vanderver[22], Matt Velinder[18], Dave Viskochil[18], Tiphanie P. Vogel[17], Colleen E. Wahl[14], Stephanie Wallace[15], Nicole M. Walley[28], Chris A. Walsh[16], Melissa Walker[16], Jennifer Wambach[27], Jijun Wan[24], Lee-kai Wang[24], Michael F. Wangler[34], Patricia A. Ward[30], Daniel Wegner[27], Mark Wener[15], Tara Wenger[24], Katherine Wesseling Perry[24], Monte Westerfield[35], Matthew T. Wheeler[26], Jordan Whitlock[25], Lynne A. Wolfe[14], Jeremy D. Woods[24], Shinya Yamamoto[34], John Yang[14], Muhammad Yousef[14], Diane B. Zastrow[26], Wadih Zein[14], Chunli Zhao[26] and Stephan Zuchner[20]

[14]National Institutes of Health, Undiagnosed Diseases Program Clinical Site, Bethesda, MD, USA. [15]University of Washington and Seattle Children's Hospital Clinical Site, Seattle, WA, USA. [16]Harvard-affiliated Boston Children's Hospital, Massachusetts General Hospital, Brigham and Women's Hospital, and Brigham Genomics Medicine Clinical Site, Boston, MA, USA. [17]Baylor College of Medicine, Clinical Site, Houston, TX, USA. [18]University of Utah Clinical Site, Salt Lake City, UT, USA. [19]Stanford University Clinical Site, Stanford, CA, USA. [20]University of Miami Clinical Site, Miami, FL, USA. [21]Washington University of Saint Louis, Clinical Site, Saint Louis, MO, USA. [22]Children's Hospital of Philadelphia or University of Pennsylvania Clinical Site, Philadelphia, PA, USA. [23]Vanderbilt University Clinical Site, Nashville, TN, USA. [24]University of California, Los Angeles, Clinical Site, Los Angeles, CA, USA. [25]University of Alabama Coordinating Center, Birmingham, AL, USA. [26]Stanford University Clinical Site, Stanford, CA, USA. [27]Washington University of Saint Louis, Clinical Site, Saint Louis, MO, USA. [28]Duke University Clinical Site, Durham, NC, USA. [29]Mayo Clinic Metabolomics Core, Rochester, MN, USA. [30]Baylor Genetics Sequencing Core, Houston, TX, USA. [31]Harvard Medical School Coordinating Center, Boston, MA, USA. [32]Columbia University Clinical Site, New York City, NY, USA. [33]Washington University of Saint Louis, Model Organism Screening Center, Saint Louis, MO, USA. [34]Baylor College of Medicine, Model Organism Screening Center, Houston, TX, USA. [35]University of Oregon, Model Organism Screening Center, Eugene, OR, USA.